

A series of COVID-19 autopsies with clinical and pathologic comparisons to both seasonal and pandemic influenza

Phillip McMullen^{1*} , Peter Pytel¹, Alexis Snyder¹, Heather Smith¹, Jasmine Vickery¹, James Brainer¹, Robert Guzy² , David Wu², Nathan Schoettler², Ayodeji Adegunsoye², Anne Sperling², John Hart¹, Lindsay Alpert¹, Anthony Chang¹, Sandeep Gurbuxani¹, Thomas Krausz¹, Aliya N Husain¹ and Jeffrey Mueller¹

¹Department of Pathology, University of Chicago Medical Center, Chicago, IL, USA

²Department of Medicine, Section of Pulmonary and Critical Care Medicine, University of Chicago Medical Center, Chicago, IL, USA

*Correspondence to: Phillip McMullen, Department of Pathology, University of Chicago Medical Center, 5841 S Maryland Ave, Chicago, IL, USA.

E-mail: phillip.mcmullen@uchospitals.edu

Abstract

Autopsies of patients who have died from COVID-19 have been crucial in delineating patterns of injury associated with SARS-CoV-2 infection. Despite their utility, comprehensive autopsy studies are somewhat lacking relative to the global burden of disease, and very few comprehensive studies contextualize the findings to other fatal viral infections. We developed a novel autopsy protocol in order to perform postmortem examinations on victims of COVID-19 and herein describe detailed clinical information, gross findings, and histologic features observed in the first 16 complete COVID-19 autopsies. We also critically evaluated the role of ancillary studies used to establish a diagnosis of COVID-19 at autopsy, including immunohistochemistry (IHC), *in situ* hybridization (ISH), and electron microscopy (EM). IHC and ISH targeting SARS-CoV-2 were comparable in terms of the location and number of infected cells in lung tissue; however, nonspecific staining of bacteria was seen occasionally with IHC. EM was unrevealing in blindly sampled tissues. We then compared the clinical and histologic features present in this series to six archival cases of fatal seasonal influenza and six archival cases of pandemic influenza from the fourth wave of the ‘Spanish Flu’ in the winter of 1920. In addition to routine histology, the inflammatory infiltrates in the lungs of COVID-19 and seasonal influenza victims were compared using quantitative IHC. Our results demonstrate that the clinical and histologic features of COVID-19 are similar to those seen in fatal cases of influenza, and the two diseases tend to overlap histologically. There was no significant difference in the composition of the inflammatory infiltrate in COVID-19 and influenza at sites of acute lung injury at the time of autopsy. Our study underscores the relatively nonspecific clinical features and pathologic changes shared between severe cases of COVID-19 and influenza, while also providing important caveats to ancillary methods of viral detection.

Keywords: COVID-19; autopsy; viral pneumonia; diffuse alveolar damage; viral sepsis; influenza

Received 30 December 2020; Revised 25 February 2021; Accepted 6 April 2021

No conflicts of interest were declared.

Introduction

The disease caused by the novel variant of SARS-coronavirus (known as COVID-19) continues to be a global health emergency with over 109,000,000 confirmed infections [1]. At the time of this report, the United States alone has over 27,000,000 confirmed cases and over 500,000 deaths [2]. As COVID-19 is an infectious disease with high transmissibility, autopsies in positive patients require special precautions [3–5], and there are several case reports and autopsy series

detailing pathologic findings across a number of institutions [3–24]. While these procedures are often limited to cardiovascular and pulmonary examination [6–10,25], many of the emerging reports are more comprehensive and include analysis of multiple organ systems [11–24]. The principal site of injury for COVID-19 is the lungs, and pulmonary findings include many nonspecific findings such as edema, chronic inflammation, hyaline membranes, acute-to-organizing diffuse alveolar damage (DAD), and superimposed bronchopneumonia [4–10]. There are rare reports of cardiac involvement,

including eosinophilic myocarditis [21], but the majority of the cardiovascular findings described are minimal and nonspecific [8,12,24,25]. Thrombotic complications are increasingly described as a potential unique aspect of COVID-19 [26–28], but disseminated intravascular coagulation secondary to viral infection is a well-described phenomenon that has been seen across a number of severe viral infections [29]. Reports of nonpulmonary findings at autopsy, including kidney [13,14], spleen [18], and liver [19], are also emerging in the literature. Examination of organs apart from the lungs has been largely guided by clinical manifestations in severe infections (such as rising liver function tests and renal failure), but the significance of the reported findings in these organs remains largely uncertain given the overall nonspecific nature of the findings and lack of comparison to other viral infections.

Herein, we describe a novel autopsy protocol used to perform comprehensive autopsies on COVID-19 patients and report the first 16 autopsies. The cumulative pathologic findings identified in the lungs, heart, liver, spleen, kidneys, lymph nodes, muscle, and peripheral nerves are described. In addition, we critically evaluate the role of ancillary methods of viral detection including immunohistochemistry (IHC), chromogenic *in situ* hybridization (ISH), and electron microscopy (EM). In order to provide more appropriate context to the pathologic changes noted in these cases, and to assess for significant differences compared to other fatal viral infections, we also performed direct comparisons of our COVID-19 cases to archival cases of fatal influenza infection to include both seasonal strains (spanning from 2015 to 2018) and archival cases of pandemic influenza during the fourth wave of the ‘Spanish Flu’ in the winter of 1920.

Methods

Protocol development and autopsy procedure

We developed a modified autopsy protocol (see supplementary material, File S1) to provide protection from accidental transmission of COVID-19, and to streamline the autopsy procedure such that the exposure time was limited. All included cases were consented for autopsy by the appropriate patient representative(s). All research performed herein was approved by the IRB at our institution as a ‘Research on Decedents’ protocol. We utilized a team of three to four individuals who were all experienced at autopsy and trained in our emerging infectious disease protocol (AIS, PP, JM, PM, HS, and JV). The team was organized as follows: There were one to two prosectors

working to remove the organs; another prosector weighed, cleaned, and sectioned the organs; and the last prosector took photographs, recorded findings, and documented weights. All policies were reviewed and approved by our institution’s infection control. All autopsy procedures followed College of American Pathologists (CAP) and Center for Disease Control (CDC) guidelines, and were comparable to prior publications [3–6].

The specimens collected included trachea, lungs, heart, liver, spleen, lumbar plexus (peripheral nerve), skeletal muscle (psoas), lymph nodes, and kidneys. Incidental pathologies discovered at the time of autopsy were also sampled on every case. In some cases, nasopharyngeal biopsies were performed using a punch biopsy needle. Only 1 of the 16 cases was limited to the heart and lungs. None of the patients underwent brain or spinal cord assessment due to the risk of aerosolized particles generated by the saw. All of the saved organs were immediately fixed in formalin for >72 h prior to sectioning for histology. Histologic sections included the following: Peripheral, middle, and hilar lung sections for each lobe from both lungs; apex/base sections of myocardium from each ventricle and the interventricular septum; representative cortex, medulla, and pelvis from each kidney; representative sections of each liver lobe and the spleen; sections containing any lymph nodes; and a section of any additional pathologies found during the autopsy. Select immunohistochemical studies were performed using Leica (Wetzlar, Germany) automated instruments in the Department of Pathology at the University of Chicago Medical Center.

Validating and assessing the utility of ancillary methods of viral detection

Three methods of viral identification were trialed across our series. IHC targeting the viral nucleocapsid was performed using a mouse monoclonal antibody produced by Thermo-Fisher Scientific (Cat. No. MA1-7404; Waltham, MA, USA). ISH was performed using the SARS-CoV-2 RNA probe produced by Advanced Cellular Diagnostics (Cat. No. 848568; Newark, CA, USA). A positive control for these two methods was made using formalin-fixed SARS-CoV-2-infected VERO cells obtained from the University of Chicago Human Tissue Resource Laboratory (HTRL; Lemont, IL, USA). The suspension of formalin-fixed COVID-19-infected VERO cells was used to create a cell block, which was sectioned into 5 μ m slides and subsequently tested with each of the commercial reagents. In addition to these commercial means of viral detection, we evaluated the utility of EM performed

on both 'blind' selections of tissue selected at autopsy and targeting regions of IHC/ISH positivity by dissecting tissue of interest from paraffin blocks.

Quantitative IHC of inflammation

Quantification of IHC stains was performed using Philips Digital Pathology Software (DPS; Amsterdam, The Netherlands), QuPath [30], and GraphPad Prism (San Diego, CA, USA). In brief, slides were first scanned into Philips DPS and geographically linked. Slides stained with CD3, CD8, and CD20 IHC markers were evaluated at various magnifications (CD4 was derived mathematically from the proportion of CD8:CD3 T-cells) and representative screenshots were saved. These geographically linked screenshots were then assessed using QuPath. Regions of interest (ROIs) were defined as areas of pathologic change with increased IHC staining within lung parenchyma. Lymph nodes and apparent nodal tissue were not considered in this analysis. The ROIs were drawn and duplicated so that they were matched to the other corresponding stains. The end result was that the exact

same areas were being evaluated for each stain. The positive pixel area in each ROI was used to derive a ratio of CD8:CD3 cells, and to calculate the estimated CD4:CD8 ratios. The resulting data were averaged both by results per patient and across all replicates for each stain. The averages and distributions of results were graphed and statistically interrogated using GraphPad Prism. The statistics were performed using unpaired Student's *t*-tests with Welch's correction (for comparison of means with unequal distributions). Results of $p < 0.05$ were considered statistically significant.

Results

Clinical information for COVID-positive cases

Pertinent clinical information and select laboratory studies for COVID-19 patients are summarized in supplementary material, Table S1. All patients were tested for COVID-19 by nasal swab prior to death, and all were positive. The average patient age was 65 years,

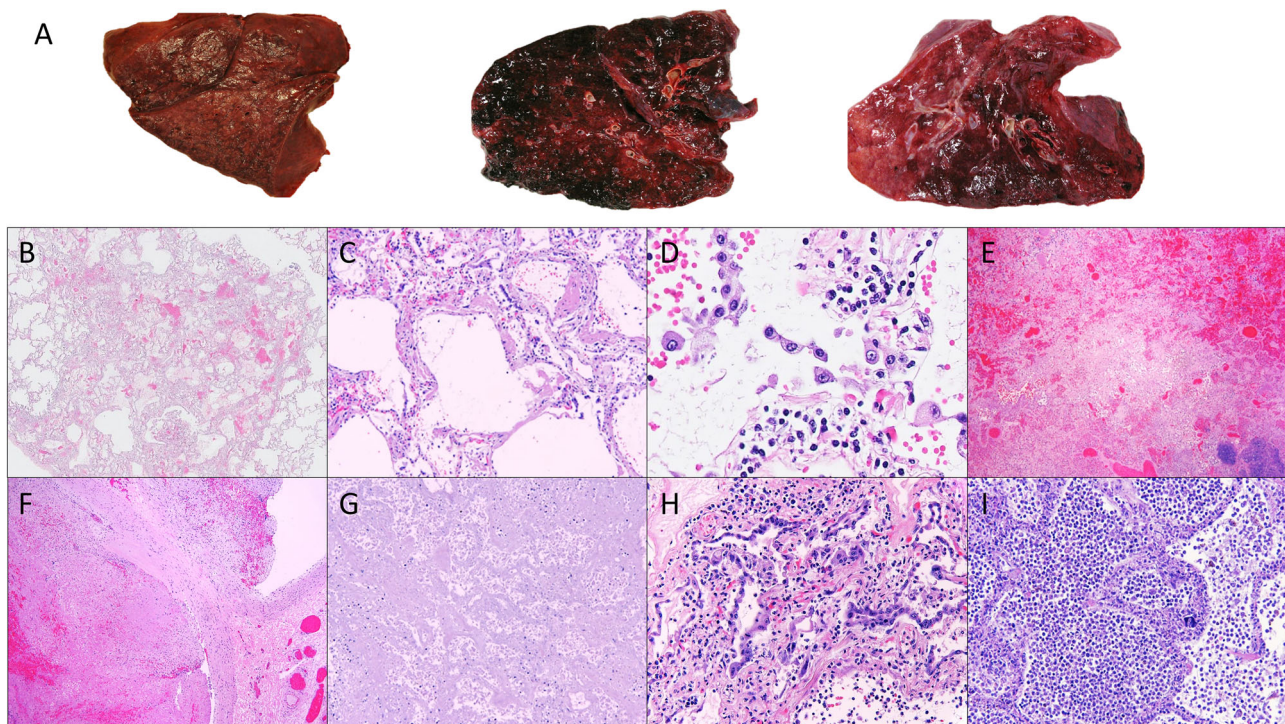


Figure 1. Representative gross and microscopic findings from COVID-19 autopsies. (A) Spectrum of representative gross changes including diffuse consolidation and variable amounts of hemorrhage. (B,C) DAD ($\times 10$ and $\times 100$ magnification, respectively). (D) Interstitial capillary with inflammation ($\times 400$) and detachment of alveolar pneumocytes. (E) Hemorrhage ($\times 10$ magnification). (F) Thrombosis ($\times 10$ magnification). (G) Infarction ($\times 10$ magnification). (H) Reactive, detached pneumocytes ($\times 200$ magnification). (I) Superimposed bacterial pneumonia ($\times 100$ magnification). All magnifications represent total magnification.

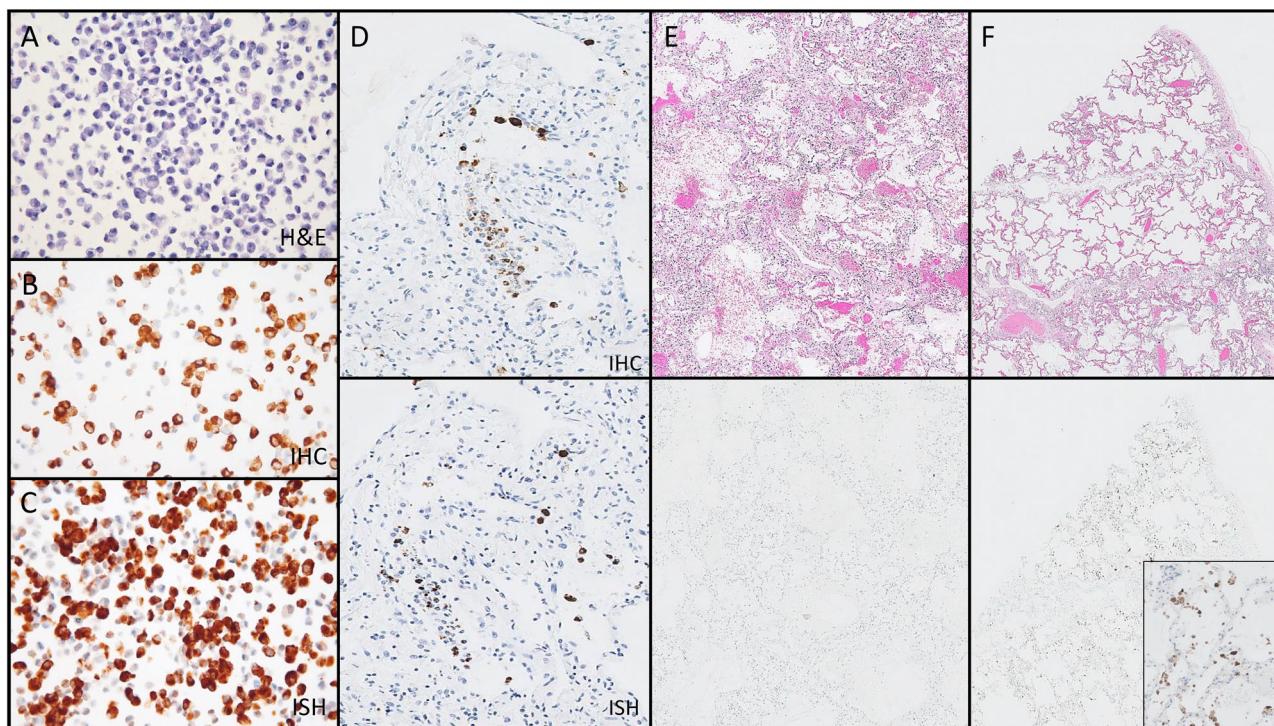


Figure 2. Assessment of IHC and ISH for the identification of SARS-CoV-2-infected cells. (A–C) Positive control cell block made of SARS-CoV-2-infected VERO cells, with hematoxylin and eosin (A, $\times 200$ magnification), IHC using the Thermo-Fisher Scientific monoclonal antibody (B, $\times 200$ magnification), and RNAScope ISH (C, $\times 200$ magnification). (D) Paired region analysis showing the distribution of virus-infected cells is comparable between IHC (upper panel) and ISH (lower panel) ($\times 100$ magnification). (E) Paired region analysis showing that histopathologic changes associated with COVID-19 (upper panel) may be negative for virus-infected cells by IHC (lower panels) ($\times 20$ magnification). (F) Paired region analysis showing relatively bland areas (upper panel) may have many virus-infected cells by IHC (lower panel) (F, $\times 20$ magnification; inset $\times 200$ magnification). All magnifications represent total magnification.

and the majority of cases were female (56%). Eleven out of 16 patients were African-American (69%), 3 patients were Hispanic (19%), and 2 patients were Caucasian (13%). Fourteen of 16 patients (88%) presented with cardiopulmonary symptoms and 15 patients (94%) had abnormal chest imaging on admission. The average length of admission was 15.3 days (range 2–59), and 11 of 16 (69%) patients were intubated and mechanically ventilated. Nine of 16 patients (56%) had sputum or endotracheal aspirates performed during admission, and 4 of those 9 (44%) were found to be growing significant pathogens. Of note, D-dimers were drawn on 15 of 16 (94%) COVID-19 patients and all of the 15 D-dimers were elevated, with 8 of 15 (53%) being >20 . High-sensitivity troponin was drawn in 14 of 16 cases, with 9 of 14 (64%) showing some degree of elevation and 5 of 14 (36%) showing significant elevations. Eight patients were retested for SARS-CoV-2 by nasopharyngeal swab polymerase chain reaction (PCR) prior to starting the autopsy and all but one were still positive. The single patient who tested

negative prior to autopsy had a prolonged hospital course with over a month interval between initial testing and autopsy.

Clinical information for influenza-positive cases

Six representative fatal seasonal influenza cases and six fatal pandemic influenza cases were pulled from our institution's archives for comparison to COVID-19 cases. All included cases were consented for autopsy by the appropriate patient representative(s), and all research was approved by our institution's IRB through a Research on Decedents protocol. The seasonal influenza cases spanned from 2015 to 2018, and thus represented heterogeneous influenza strains. The six pandemic influenza autopsy cases were from the fourth wave of the Spanish Flu and were performed in the winter of 1920. Blocks were not available for the pandemic influenza cases and evaluation was therefore limited to histomorphology. Many of the targeted laboratory procedures performed on all of the COVID-19

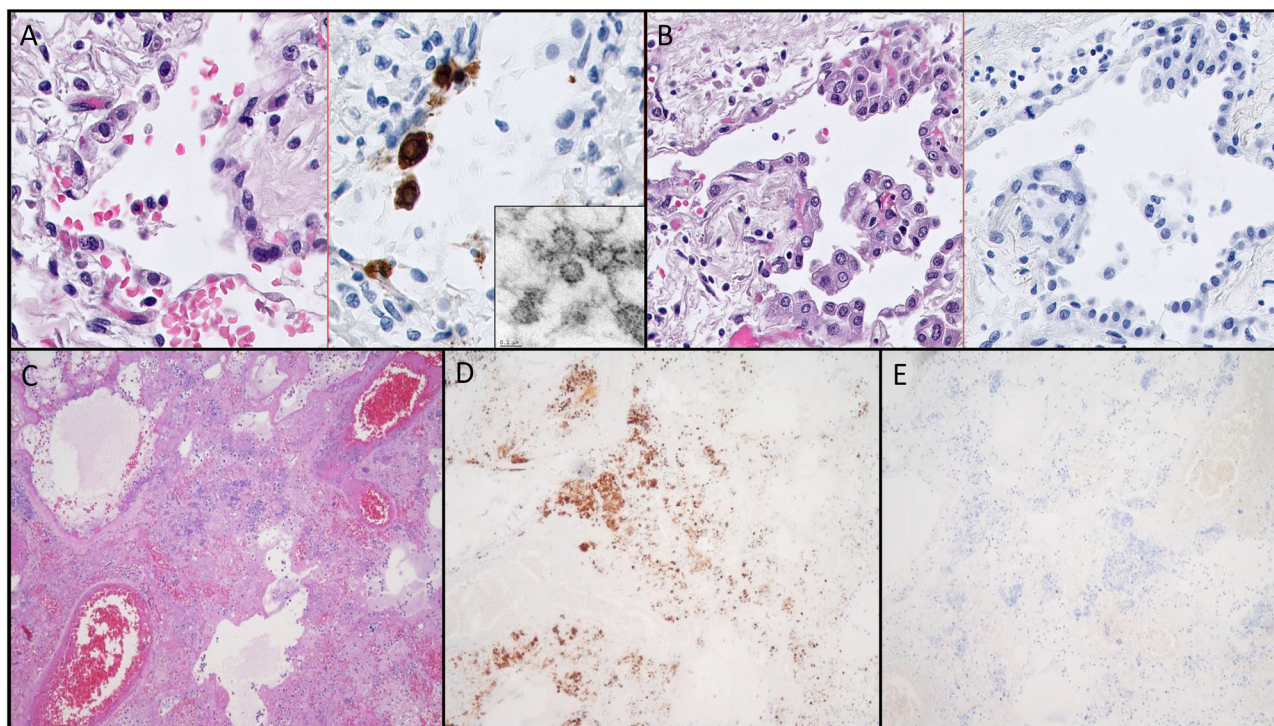


Figure 3. The nonspecific cytomorphology of SARS-CoV-2-infected cells in human tissues and demonstration of cross-reactivity with IHC reagents. (A) Hematoxylin and eosin (H&E)-stained section (left) with paired IHC (right) of virus-infected cells showing cytoplasmic vacuolization and reactive nuclear changes in infected cells ($\times 600$ magnification). Tissue dissected from this IHC-positive region of the paraffin block demonstrates candidate virion-like particles (inset, EM, $\times 80,000$). (B) IHC of a group of cells from the same case (left H&E, right IHC) with identical cytomorphologic features which are negative for virus by IHC ($\times 400$ magnification). (C–E) Demonstration of nonspecific staining of bacteria by IHC in a case of necrotizing bacterial pneumonia and influenza from 2015. (C) H&E-stained image of the region of positive staining ($\times 100$ magnification). (D) Positive staining of bacteria and bacteria-laden macrophages by IHC ($\times 200$ magnification). (E) Negative ISH staining of the same region ($\times 200$ magnification). All magnifications represent total magnification.

patients were not performed on influenza patients. Results which were available for review are shown in supplementary material, Table S2 (note that clinical information for the pandemic influenza patients was severely limited due to a lack of records and lack of modern laboratory testing platforms). The average patient age was less than that of the COVID-19 patients, with seasonal influenza patients averaging 46 years of age and pandemic influenza patients averaging 37 years of age (compared with 65 years for COVID-19). The average length of admission was also shorter for seasonal influenza patients (3.5 versus 15.3 days for COVID-19). Three of the seasonal influenza patients had concurrent infections, one viral (human metapneumovirus) and two bacterial (both methicillin-sensitive *Staphylococcus aureus*). D-dimers were drawn on three of six (50%) seasonal influenza patients, and all three were >20 . One of the seasonal influenza patients who did not have a D-dimer result

was actively treated for pulmonary embolism by heparin drip. Thus, cumulatively, four of six (67%) influenza patients had either laboratory indicators or clinical evidence of thrombosis. Troponin assays were performed on five of six seasonal influenza patients, with three of five (60%) showing some degree of elevation and one of five (20%) showing significant elevation.

Major COVID-19 autopsy findings

The lungs were grossly abnormal in nearly all of the COVID-19 cases (Figure 1A and supplementary material, Table S3). The most common gross finding was consolidation, with 7 of 16 (44%) cases exhibiting diffuse consolidation and 2 cases (13%) exhibiting focal consolidation. Other somewhat frequent findings were hemorrhagic appearing parenchyma (present in 3/16, 18%) and edema (present in 2/16, 12%). Fibrosis was

present in one case (6%), and one case exhibited findings consistent with metastatic carcinoma. Only one case (case 9) exhibited no significant consolidation or hemorrhage, but both lungs in this case were still found to be heavy compared to age-matched controls. All of the lung weights were abnormal, with an average weight of 841 g on the right side and 727 g on the left.

There were a number of histologic changes identified in the lungs across the 16 examined cases (Figure 1B–I and supplementary material, Table S4). DAD was present in 12 of 16 (75%) cases and presented as a spectrum from early-to-organizing DAD. Organizing thrombi were identified in 6 of 16 (38%) cases and infarction secondary to thrombosis was present in 4 of 16 (25%) cases. Interstitial inflammation in the alveolar capillaries was identified in several cases (Figure 1D). Superimposed infections were present in 9 of 16 (56%) cases, the most common being bacterial pneumonia (6/16 cases, 38%) and aspiration pneumonia (3/16 cases, 19%). Scattered microscopic thrombi were identified in the pulmonary capillaries in

10 of 16 (63%) cases, and nine of these cases were evaluated by CD61 immunostaining, which confirmed that the thrombi were platelet-rich.

Prominent reactive pneumocytes were present in 13 of 16 (81%) cases (Figure 1D,H). Cytologically, these cells were enlarged with vacuolated, amphiphilic cytoplasm, and exhibited variably large nucleoli with open to vesicular chromatin (Figure 1D). Occasionally, these cells were multinucleated, and tended to be present as linear strips floating in alveolar spaces. These cells appeared morphologically similar to histologic changes previously identified both in cases of SARS infections and influenza [31–34]. A timeline of the histopathologic changes seen in the lungs over various lengths of admission is shown in supplementary material, Table S5.

No disease-specific alterations were identified in any of the COVID-19 hearts, kidneys, liver, spleen, or lymph nodes. Detailed microscopic descriptions of these organs can be found in supplementary material, Table S4. In brief, the most common histologic findings related to the heart were myocyte hypertrophy

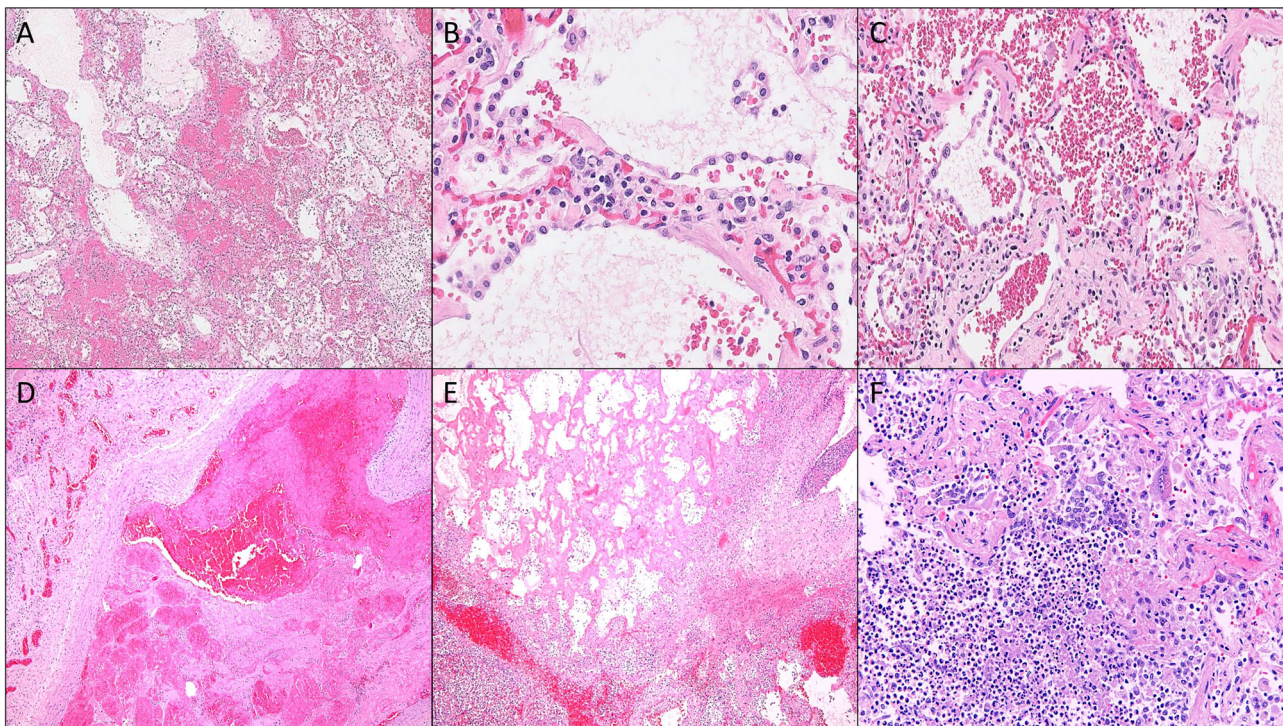


Figure 4. Representative histologic findings in cases of fatal seasonal influenza taken from archival specimens. (A) DAD histologically indistinguishable from COVID-19 ($\times 50$ magnification). (B) Interstitial inflammation with reactive, detached pneumocytes ($\times 400$ magnification). (C) Reactive, detached pneumocytes in a background of alveolar hemorrhage ($\times 200$ magnification). (D) Thrombosis ($\times 50$ magnification). (E) Infarction ($\times 50$ magnification). (F) Superimposed bacterial pneumonia ($\times 200$ magnification; note the presence of prominent and occasionally multinucleated pneumocytes).

and interstitial fibrosis, both of which were present in 3 of 16 cases (19%). Thrombotic microangiopathy was identified in 5 of 15 kidneys (33%), and acute tubular injury/necrosis was identified in 4 cases (27%). In addition, basophilic casts were present in 5 of 15 cases (33%), which may be medication related. Other renal findings most often correlated with underlying medical comorbidities, such as diabetes (5/15 cases, 33%) and hypertension/arterionephrosclerosis (4/15 cases, 27%). The livers showed a range of histologic changes that were related to the patients' underlying conditions, including the presence of minimal to mild macrovesicular steatosis in 9 of 15 cases (60%). Nearly all of the spleens showed some depletion of the white pulp and congestion of the sinuses, with a small number (3/15, 20%) exhibiting increased hemophagocytosis in the sinusoids. A significant percentage of cases (11/16 or 69%) showed depleted follicles with reduced germinal center formation along with expansion of the sinuses by histiocytes (positive for CD68 and CD163, with no staining of CD20 and CD3) in the hilar and peribronchial lymph nodes. Five of 16 lymph nodes (31%) exhibited significantly increased hemophagocytosis, and 2 (13%) also

showed occlusion of small blood vessels by platelet-rich thrombi (assessed by CD61).

Viral detection by ancillary methods

All commercial reagents tested in our study reacted appropriately with our positive control cell block of COVID-19-infected VERO cells (Figure 2A–C). The monoclonal antibody from Thermo-Fisher Scientific demonstrated convincing staining of individual cells in several cases; however, the distribution of virus appeared to be patchy in tissue sections. The patterns of staining between IHC and ISH were largely congruent (Figure 2D). Interestingly, the infected cells were more abundant in areas without significant pathologic change (Figure 2E,F). Both IHC and ISH demonstrated that a subset of the reactive appearing pneumocytes were positive for SARS-CoV-2. However, both infected and noninfected reactive pneumocytes exhibited cytoplasmic vacuolation, amphiphilic cytoplasm, and occasional reactive nuclear changes, making it impossible to distinguish infected versus noninfected cells by light microscopy alone (Figure 3A,B).

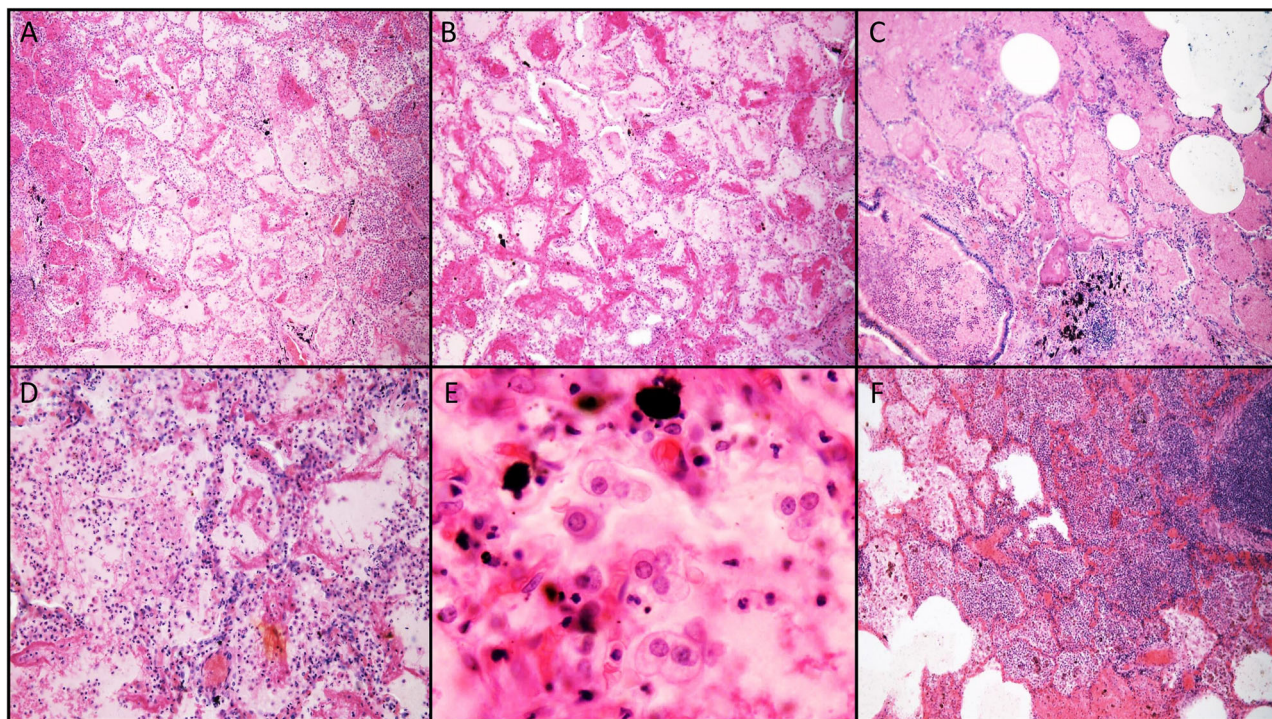


Figure 5. Representative histologic findings in cases of fatal pandemic influenza taken from archival specimens. (A,B) DAD ($\times 100$ magnification). (C) DAD, edema, and hemorrhage adjacent to an airway containing inflammatory mucus ($\times 100$ magnification). (D) Interstitial capillary inflammation ($\times 200$ magnification). (E) Reactive pneumocytes exhibiting nucleoli and cytoplasmic vacuoles, similar to those seen in seasonal influenza and COVID-19 ($\times 400$ magnification). (F) Superimposed bacterial pneumonia ($\times 100$ magnification).

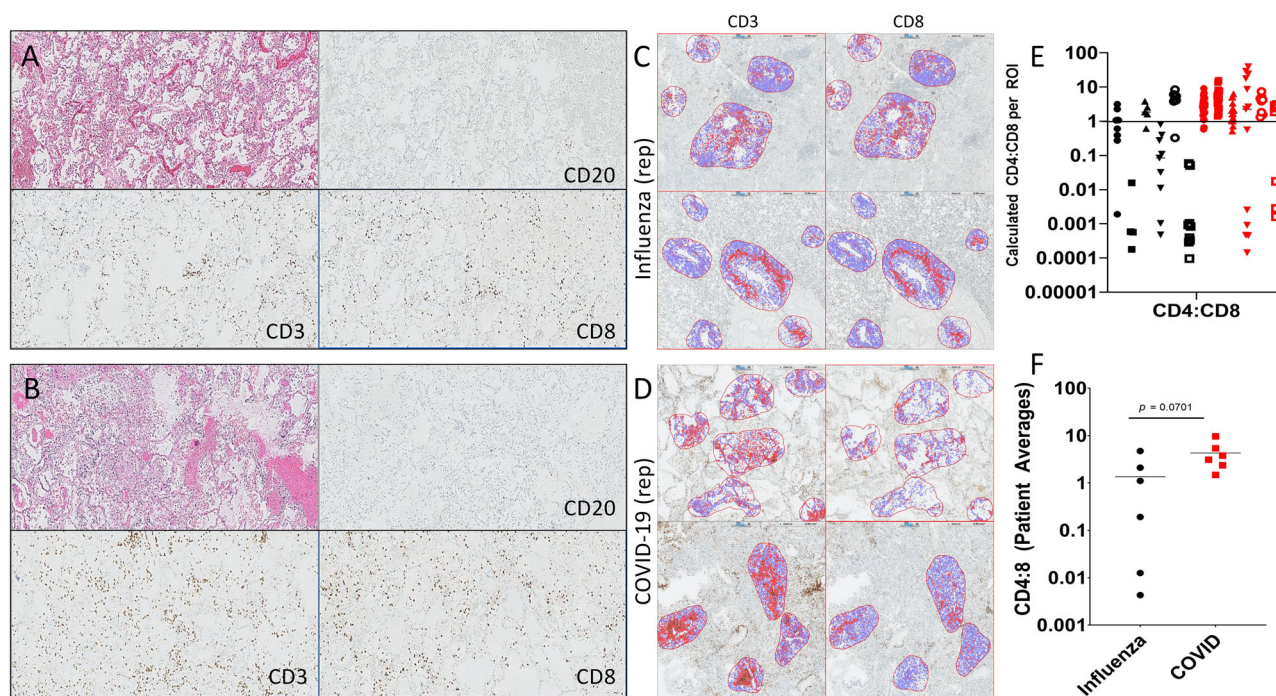


Figure 6. Quantitative assessment of inflammation in COVID-19 and seasonal influenza. Representative paired regions showing hematoxylin and eosin (H&E) staining along with CD20, CD8, and CD3 immunostains (clockwise from H&E) for (A) influenza and (B) COVID-19. The distribution of T-cells and relative abundance of CD8-positive cells relative to CD3 is comparable. (C,D) Representative ROI analysis for CD3 and CD8 immunostains in a case of (C) fatal influenza and (D) COVID-19. (E,F) Graphical representation of individual CD4:CD8 ratios per ROI (E) and cumulative CD4:CD8 ratios per patient (F). Note that there is no significant difference of CD4:CD8 ratios between COVID-19 and influenza, although there is a trend toward higher CD4:CD8 for COVID-19. In Figure 1E, individual patients are identified by a unique shape on the graph for each disease.

Instances of nonspecific staining were noted with the IHC antibody used in our study. Two cases of influenza from 2015 with a superimposed bacterial infection stained strongly and convincingly for SARS-CoV-2 (Figure 3C–E). The use of simple special stains, such as the tissue Gram stain and Prussian blue stains, was able to resolve this dilemma in retrospect, and ISH did not cross-react with bacteria in the same section of tissue (Figure 3E). Blind sampling of lung tissue for EM was unable to demonstrate convincing virion structures across 10 sampled cases (which amounted to approximately 25 separate EM grids). Using IHC and ISH to direct sampling of paraffin-embedded tissue for EM did reveal occasional ‘virion-like’ particles in cells morphologically consistent in location and appearance to viral infected cells (Figure 3A, inset). These particles exhibited a size between 80 and 120 nm, and contained internal dot-like structures morphologically resembling virions [35]. However, as the description of virion ultrastructure is somewhat nonspecific, and there were numerous mimics of virions identified across the blind sections we assessed, we defer from definitively stating

the structures identified even in these targeted areas represent real virions.

Pathologic comparison of COVID-19 to fatal influenza

The histologic features of influenza infection were first reviewed to guide our comparison to COVID-19 [33,34]. There was substantial overlap between influenza and COVID-19 in terms of histologic findings in the lungs (Figures 4 and 5). DAD was an abundant finding in cases of influenza, present in 7 of 12 cases (58%), as was hemorrhage (8/12, 67%) (Figures 4 and 5, and supplementary material, Table S2). There was an apparent enrichment for hemorrhage in influenza cases (67% versus 31%), and this difference trended toward significance ($p = 0.07$, chi-squared). Superimposed infectious processes were also present in 10 of 12 (83%) cases, including all of the pandemic influenza cases. Reactive pneumocytes were identified in several sections of both seasonal and pandemic influenza cases (Figures 4B,C,F and 5E). These cells shared similar features to COVID-19, such as cytoplasmic

vacuolation, open chromatin, and prominent nucleoli and were more-or-less indistinguishable from those observed in COVID-19. CD61 staining revealed the presence of platelet-rich thrombi in cases of influenza, but the overall abundance of platelet thrombi was significantly lower in influenza than in COVID-19 infection, although these results are discussed elsewhere [36].

Similar to COVID-19 infection, patchy interstitial CD3+ T-cells were the predominant inflammatory cells in seasonal influenza, and were found to be a mix of CD8 and CD4 (Figure 6A–D), with rare CD20+ B-cells also identified. Quantitative IHC was performed using the six seasonal influenza cases and six representative COVID-19 cases exhibiting typical findings. The difference in the mean CD4:CD8 ratios was not significant (Figure 6C–F), although COVID-19 seemed to have an overall trend for higher CD4:CD8 ratios than did influenza. It is worth noting that the ratio of T-cell subsets was quite variable across different ROIs, even within the same patient for both COVID-19 and influenza. A spatially dependent pattern of recruitment at different sites within the lung has been previously reported to occur in influenza infection [34], but to our knowledge such studies have not yet been performed for coronavirus infections. Lymph nodes had been sampled in three of the six influenza cases, and all showed depleted follicles with some component of sinus histiocytosis. Control lymph nodes from cancer resections also demonstrated a degree of sinus histiocytosis, which was often associated with anthracosis, a common finding in the thoracic lymph nodes of city dwellers in general. Therefore, the significance of the findings in the lymph nodes of COVID-19 patients (i.e. depletion and sinus histiocytosis) is questionable, and overall there were no striking differences between the groups.

Discussion

In our comparative case series, we found that most of the histologic features described for COVID-19 also occurred in both seasonal and pandemic influenza cases. In addition, there was a great degree of clinical overlap among COVID-19 and influenza patients in our study, most notably the need for mechanical ventilation in a substantial subset of both groups and the presence of bacterial superinfections. These commonalities may of course obscure more subtle disease-specific alterations, but an important conclusion of our data is that these nonspecific complications occur at similar rates in both severe COVID-19 and influenza,

indicating at least some stereotypical clinical progression in severe cases of both diseases. One of the substantial clinical differences between the groups was the average age, with the average COVID-19 patient being 65 years compared to 46 years for seasonal influenza and 34 years for pandemic influenza.

With regard to histologic features, influenza cases tended to exhibit hemorrhagic changes more frequently than COVID-19, but this was more of a trend than a statistically significant difference in our dataset. Although thrombosis has been described as a somewhat unique feature of COVID-19 infection relative to other infections, thrombi were not especially specific to the COVID-19 patients in our study, as elevated D-dimers were found in the majority of both COVID-19 and seasonal influenza patients studied. As mentioned above, a prior report did demonstrate that COVID-19 cases exhibit significantly higher degrees of CD61-rich microthrombi in the pulmonary vasculature compared to influenza [36]. That same study also demonstrated that microthrombi are seen across the spectrum of both infectious and noninfectious causes of DAD, and there were several other conditions in that study which resulted in more microthrombi than COVID-19. Microthrombi and thrombosis at large are recognized components of both severe viral infections and DAD [30,36] and, as autopsy cases naturally reflect more severe cases of infection, it is possible that such studies naturally enrich patients with severe thrombotic complications. Overall, the coagulopathic changes seen in COVID-19 autopsies appear to be not entirely specific to the disease when compared to other severe infectious diseases [37,38].

While the differences in immune infiltrate (i.e. the mean CD8:CD4 ratio) present in the lungs of COVID-19 patients were not significantly different to influenza cases in our study, there was a trend for higher CD4:CD8 ratios in COVID-19, a finding which has been detailed previously [39]. The limited number of cases assessed by this method along with the inability to control for patient-to-patient variabilities may be confounding factors to this sort of analysis. Overall, the composition of the inflammatory infiltrate merits further investigation with more sensitive and specific methods in more controlled settings, such as those performed previously for influenza [34]. Given that the principal function of CD4 T-cells is one of cytokine production and immune regulation [40], their apparent enrichment in COVID-19 relative to influenza infection may be related to pertinent pathophysiologic differences between the two infections and should be studied further. As it stands, our data in regards to the immune infiltrate only demonstrate that typing of T-cells or other leukocytes is not likely to provide diagnostic utility in the autopsy setting.

Our comprehensive approach relied on the input of expert diagnosticians across many different subspecialties of pathology for all of the organ systems assessed in our COVID-19 cohort, which adds credence to both positive and negative findings across all the organ systems assessed. Both our COVID-19 and seasonal influenza patient populations were predominantly African-American and, to our knowledge, no studies comparing the pathology and laboratory data of COVID-19 and influenza have been performed in predominantly African-American populations. In addition, the prior autopsy studies of African-American patients with COVID-19 have been limited in nature [8] despite African-Americans bearing a disproportionate burden of morbidity in the pandemic [41]. Based on our data, the pathologic changes in African-Americans seem to be more-or-less identical to those seen in other races, with no specific histomorphologic alterations apparent in our series. The disproportionate burden of mortality observed in a prior study may therefore be multifactorial in nature [41], or at least is due to factors not apparent in routine histopathologic analysis. Lastly, the inclusion of several pandemic influenza cases for histologic analysis from the fourth wave of the Spanish Flu is also novel, and adds an important comparison given the pandemic nature of both COVID-19 and the Spanish Flu. While the autopsy findings in Spanish Flu and influenza have been compared to COVID-19 before [42], to our knowledge, ours is the first to incorporate the histologic findings from pandemic influenza, rather than relying on the reported findings in the historical autopsy documents. Lastly, our comprehensive analysis was coupled with a critical assessment of three ancillary methods of viral detection for SARS-CoV-2. While our data demonstrate that ancillary techniques are able to identify virus-infected cells and may be useful in establishing the diagnosis of COVID-19 infection (similar to prior reports [32,43]), there are clear pitfalls to these methods not highlighted by prior studies. The majority of IHC and ISH-directed viral staining occurred in areas with relatively minimal pathologic changes, thus targeting areas of active lung injury alone may miss the virus-infected cells. In addition, in cases of superimposed bacterial infections (which were present in the majority of both COVID-19 and influenza patients), there may be cross-reactivity with some bacterial species using some IHC reagents, potentially leading to false-positive results when using IHC alone. ISH may be a useful mechanism to resolve diagnostic dilemmas, but this method requires laboratory expertise and special reagents which may not be as widely available as those used in IHC. Special stains such as Gram stain and Prussian Blue were employed with ease in our study to discriminate non-specific staining from true staining seen with IHC. We, like others [35], strongly caution against the use of EM for viral

detection by either blind or targeted sampling of fixed tissue due to abundant mimics. Overall, we believe, based on our preliminary experience with these ancillary methods, that correlation between clinical studies obtained prior to death (notably nasopharyngeal PCR and/or serologic antibody tests) in conjunction with histologic findings could be sufficient to establish the diagnosis in the majority of cases even in the absence of these ancillary methods. In cases where there remains a high index of suspicion for COVID-19, but these ancillary methods and premortem testing remain negative, other methods not assessed in our study, such as quantitative PCR, could also be explored [43].

Our cumulative work adds to the growing body of knowledge of pathologic changes related to COVID-19 and appropriately contextualizes the pathologic findings present in COVID-19 infection with those seen in fatal influenza infections (both seasonal and pandemic varieties). The results demonstrate that the majority of pathologic changes observed are not specific to COVID-19, and therefore are in agreement with prior reports that the pathologic findings in both COVID-19 and influenza are similar and both are overall indistinguishable histomorphologically from other causes of DAD [44–46]. We caution that our results should not be interpreted to suggest that influenza and COVID-19 are equivalent in terms of clinical severity, or that they do not have critical pathophysiologic differences. Full evaluation of the pathophysiology of these two distinct diseases was beyond the scope of our study, which was limited to a comparison of both the clinical and histologic features seen in autopsy cases. Our study only asserts that the pathologic changes and the assessed laboratory values at the time of autopsy appear to be very similar across fatal cases of severe COVID-19 and influenza. The findings described are concordant overall with those published independently for both COVID-19 and influenza. Therefore, we believe that the findings could represent a common response to severe virus-induced lung injury, and overall reflect a stereotypical clinical and pathologic progression seen in severe viral infections.

Acknowledgements

The authors are greatly indebted to Gary Randall and the hard-working individuals at the COVID-Research Core at the University of Chicago for providing SARS-CoV-2-infected VERO cells for control tissue. We would like to thank Terri Li, Ming Cheng, and Can Gong of the Human Tissue Resource Center (HTRC) at the University of Chicago for performing

SARS-CoV-2 IHC and ISH, and Mark Lingen of the HTRC for his insights related to the validation process for both IHC and ISH. This study was funded by internal funding within the Department of Pathology.

Author contributions statement

PM, PP, TK, ANH and JM conceived the study, carried out experiments, analyzed the data, and wrote/reviewed the manuscript. HS, JV, AIS, JH, LA, AC and SG carried out experiments, analyzed the data, and wrote/reviewed portions of the manuscript. JB carried out experiments. RG, DW, NS, AA and AnS analyzed the data and reviewed the manuscript.

References

- World Health Organization. Coronavirus disease (COVID-2019) situation reports. [Accessed 29 March 2021]. Available from: <https://www.who.int/publications/m/item/weekly-epidemiological-update-on-covid-19--23-march-2021>
- Dong E, Du H, Gardner L. An interactive web-based dashboard to track COVID-19 in real time. *Lancet Infect Dis* 2020; **20**: 533–534.
- Hanley B, Lucas SB, Youd E, *et al.* Autopsy in suspected COVID-19 cases. *J Clin Pathol* 2020; **73**: 239–242.
- Iwen PC, Stiles KL, Pentella MA. Safety considerations in the laboratory testing of specimens suspected or known to contain the severe acute respiratory syndrome coronavirus 2 (SARS-CoV-2). *Am J Clin Pathol* 2020; **153**: 567–570.
- Center for Disease Control. COVID-19 post-mortem guidance. [Updated 22 November 2020, accessed 29 March 2021]. Available from: <https://www.cdc.gov/coronavirus/2019-ncov/hcp/guidance-postmortem-specimens.html>
- Barton LM, Duval EJ, Stroberg E, *et al.* COVID-19 autopsies, Oklahoma, USA. *Am J Clin Pathol* 2020; **153**: 725–733.
- Tian S, Hu W, Niu L, *et al.* Pulmonary pathology of early-phase 2019 novel coronavirus (COVID-19) pneumonia in two patients with lung cancer. *J Thorac Oncol* 2020; **15**: 700–704.
- Fox SE, Akmatbekov A, Harbert JL, *et al.* Pulmonary and cardiac pathology in African American patients with COVID-19: an autopsy series from New Orleans. *Lancet Respir Med* 2020; **8**: 681–686.
- Xu Z, Shi L, Wang Y, *et al.* Pathological findings of COVID-19 associated with acute respiratory distress syndrome. *Lancet Respir Med* 2020; **8**: 420–422.
- Konopka KE, Wilson A, Myers JL. Postmortem lung findings in an asthmatic patient with coronavirus disease 2019. *Chest* 2020; **158**: e99–e101.
- Menter T, Haslbauer JD, Nienhold R, *et al.* Post-mortem examination of COVID-19 patients reveals diffuse alveolar damage with severe capillary congestion and variegated findings of lungs and other organs suggesting vascular dysfunction. *Histopathology* 2020; **77**: 198–209.
- Buja LM, Wolf D, Zhao B, *et al.* The emerging spectrum of cardiopulmonary pathology of the coronavirus disease 2019 (COVID-19): report of 3 autopsies from Houston, Texas, and review of autopsy findings from other United States cities. *Cardiovasc Pathol* 2020; **48**: 107233.
- Yao XH, Li TY, He ZC, *et al.* A pathological report of three COVID-19 cases by minimally invasive autopsies. *Zhonghua Bing Li Xue Za Zhi* 2020; **49**: 411–417.
- Tian S, Xiong Y, Liu H, *et al.* Pathological study of the 2019 novel coronavirus disease (COVID-19) through post-mortem core biopsies. *Mod Pathol* 2020; **33**: 1007–1014.
- Su H, Yang M, Wan C, *et al.* Renal histopathological analysis of 26 postmortem findings of patients with COVID-19 in China. *Kidney Int* 2020; **98**: 219–227.
- Farkash EA, Wilson AM, Jentzen JM. Ultrastructural evidence for direct renal infection with SARS-CoV-2. *J Am Soc Nephrol* 2020; **31**: 1683–1687.
- Fu B, Xu X, Wei H. Why tocilizumab could be an effective treatment for severe COVID-19? *J Transl Med* 2020; **18**: 164.
- Xu X, Chang XN, Pan HX, *et al.* Pathological changes of the spleen in ten patients with coronavirus disease 2019 (COVID-19) by postmortem needle biopsy. *Zhonghua Bing Li Xue Za Zhi* 2020; **49**: 576–582.
- Li Y, Xiao SY. Hepatic involvement in COVID-19 patients: pathology, pathogenesis, and clinical implications. *J Med Virol* 2020; **92**: 1491–1494.
- Wichmann D, Sperhake JP, Lütgehetmann M, *et al.* Autopsy findings and venous thromboembolism in patients with COVID-19. *Ann Intern Med* 2020; **173**: 268–277.
- Craver R, Huber S, Sandomirsky M, *et al.* Fatal eosinophilic myocarditis in a healthy 17-year-old male with severe acute respiratory syndrome coronavirus 2 (SARS-CoV-2c). *Fetal Pediatr Pathol* 2020; **39**: 263–268.
- Lax SF, Skok K, Zechner P, *et al.* Pulmonary arterial thrombosis in COVID-19 with fatal outcome: results from a prospective, single-center, clinicopathologic case series. *Ann Intern Med* 2020; **173**: 350–361.
- Adachi T, Chong JM, Nakajima N, *et al.* Clinicopathologic and immunohistochemical findings from autopsy of patient with COVID-19, Japan. *Emerg Infect Dis* 2020; **26**: 2157–2161.
- Yan L, Mir M, Sanchez P, *et al.* COVID-19 in a Hispanic woman. *Arch Pathol Lab Med* 2020; **144**: 1041–1047.
- Inciardi RM, Lupi L, Zaccone G, *et al.* Cardiac involvement in a patient with coronavirus disease 2019 (COVID-19). *JAMA Cardiol* 2020; **5**: 819–824.
- Llitjos J-F, Leclerc M, Chochois C, *et al.* High incidence of venous thromboembolic events in anticoagulated severe COVID-19 patients. *J Thromb Haemost* 2020; **18**: 1743–1746.
- Bikdeli B, Madhavan MV, Jimenez D, *et al.* COVID-19 and thrombotic or thromboembolic disease: implications for prevention, antithrombotic therapy, and follow-up. *J Am Coll Cardiol* 2020; **75**: 2950–2973.
- Magro C, Mulvey JJ, Berlin D, *et al.* Complement associated microvascular injury and thrombosis in the pathogenesis of severe COVID-19 infection: a report of five cases. *Transl Res* 2020; **220**: 1–13.
- Lin GL, McGinley JP, Drysdale SB, *et al.* Epidemiology and immune pathogenesis of viral sepsis. *Front Immunol* 2018; **9**: 2147.

30. Bankhead P, Loughrey MB, Fernández JA, *et al.* QuPath: open source software for digital pathology image analysis. *Sci Rep* 2017; **7**: 16878.
31. Rockx B, Kuiken T, Herfst S, *et al.* Comparative pathogenesis of COVID-19, MERS, and SARS in a nonhuman primate model. *Science* 2020; **368**: 1012–1015.
32. Best Rocha A, Stroberg E, Barton LM, *et al.* Detection of SARS-CoV-2 in formalin fixed paraffin-embedded tissue sections using commercially available reagents. *Lab Invest* 2020; **100**: 1485–1489.
33. Shieh WJ, Blau DM, Denison AM, *et al.* 2009 Pandemic influenza A (H1N1): pathology and pathogenesis of 100 fatal cases in the United States. *Am J Pathol* 2010; **177**: 166–175.
34. Baumgarth N, Kelso A. Functionally distinct T cells in three compartments of the respiratory tract after influenza virus infection. *Eur J Immunol* 1996; **26**: 2189–2197.
35. Miller SE, Goldsmith CS. Caution in identifying coronaviruses by electron microscopy. *J Am Soc Nephrol* 2020; **31**: 2223–2224.
36. McMullen PD, Cho JH, Miller JL, *et al.* A descriptive and quantitative immunohistochemical study demonstrating platelet recruitment patterns across pulmonary infections including COVID-19. *Am J Clin Pathol* 2021; **155**: 354–363.
37. Wool GD, Miller JL. The impact of COVID-19 disease on platelets and coagulation. *Pathobiology* 2020; **13**: 1–13.
38. van Gorp ECM, Suharti C, ten Cate H, *et al.* Review: infectious diseases and coagulation disorders. *J Infect Dis* 1999; **180**: 176–186.
39. Ackermann M, Verleden SE, Kuehnel M, *et al.* Pulmonary vascular endothelialitis, thrombosis, and angiogenesis in COVID-19. *N Engl J Med* 2020; **383**: 120–128.
40. Geginat J, Paroni M, Maglie S, *et al.* Plasticity of human CD4 T cell subsets. *Front Immunol* 2014; **5**: 630.
41. Adegunsoye A, Ventura IB, Liarski VM. Association of Black race with outcomes in COVID-19 disease: a retrospective cohort study. *Ann Am Thorac Soc* 2020; **17**: 1336–1339.
42. Burkhard-Koren NM, Haberecker M, Maccio U, *et al.* Higher prevalence of pulmonary macrothrombi in SARS-CoV-2 than in influenza A: autopsy results from Spanish flu in 1918/1919 in Switzerland to coronavirus disease 2019. *J Pathol Clin Res* 2021; **7**: 135–143.
43. Sekulic M, Harper H, Nezami BG, *et al.* Molecular detection of SARS-CoV-2 infection in FFPE samples and histopathologic findings in fatal SARS-CoV-2 cases. *Am J Clin Pathol* 2020; **154**: 190–200.
44. Konopka KE, Nguyen T, Jentzen JM, *et al.* Diffuse alveolar damage (DAD) resulting from coronavirus disease 2019 infection is morphologically indistinguishable from other causes of DAD. *Histopathology* 2020; **77**: 570–578.
45. Harms PW, Schmidt LA, Smith LB, *et al.* Autopsy findings in eight patients with fatal H1N1 influenza. *Am J Clin Pathol* 2010; **134**: 27–35.
46. Sheng ZM, Chertow DS, Ambroggio X, *et al.* Autopsy series of 68 cases dying before and during the 1918 influenza pandemic peak. *Proc Natl Acad Sci U S A* 2011; **108**: 16416–16421.

SUPPLEMENTARY MATERIAL ONLINE

File S1. COVID-19 autopsy protocol

Table S1. Clinical data for the included COVID-19 patients

Table S2. Clinical data for the included pandemic and seasonal influenza patients

Table S3. Gross summaries for all of the assessed organs

Table S4. Histologic summaries for all of the assessed organs

Table S5. Timeline of histologic changes in the lungs of COVID-19 patients